Photoluminescence Properties of $ZnWO_4:Eu^{3+}$ Nanocrystals Prepared by a Hydrothermal Method

Qilin Dai, Hongwei Song,* Xue Bai, Guohui Pan, Shaozhe Lu, Tie Wang, Xinguang Ren, and Haifeng Zhao

Key Laboratory of Excited State Physics, Changchun Institute of Optics, Fine Mechanics and Physics, Chinese Academy of Sciences, and Graduate School of Chinese Academy of Sciences, 16 Eastern Nan-Hu Road, Changchun 130033, People's Republic of China

Received: October 12, 2006; In Final Form: March 8, 2007

$ZnWO_4:Eu^{3+}$ nanocrystals were prepared by the hydrothermal method at various temperatures and pH values. Their luminescent properties including excitation and emission processes, luminescent dynamics, and local environments surrounding Eu^{3+} ions were systemically studied. The results indicate that the particle size of the nanocrystals grows with increasing hydrothermal temperature, while it rarely changes with pH value. The excitation bands for Eu^{3+}, which are contributed by different components, shift considerably to blue with the increasing pH value. The relative intensity of blue-green emission bands caused by the tungstate groups can be greatly modified by changing the pH value, thus the white color phosphors can be obtained. There exist two symmetry sites for the $^5D_0-{}^7F_2$ emissions of Eu^{3+}, inner and surface. The former corresponds to lines with narrower inhomogeneous width and slower decay time, while the latter to the lines with broader width and faster decay time. The emissions for tungstate groups mainly originate from the charge transfer from excited 2p orbits of O^{2-} to the empty orbits of the central W^{6+} ions. On the other hand, the emissions for Eu^{3+} ions are contributed by both the charge transfer from O^{2-} to Eu^{3+} and the energy transfer from W^{6+} ions to Eu^{3+} ions. A schematic is proposed to explain the photoluminescence processes in the $ZnWO_4:Eu^{3+}$ nanocrystals.

I. Introduction

It is known that tungstate is a very important family of inorganic material that has a high potential application in various fields,[1] such as photoluminescence,[2] microwave applications,[3] optical fibers,[4] scintillator materials,[5] and so on. As a self-activating phosphor, tungstate has some advantages, e.g., high chemical stability, high average refractive index, high X-ray absorption coefficient, high light yield, short decay time, and low afterglow to luminescence. There exist two types of structure in tungstates: wolframite and scheelite. Zinc tungstate has the wolframite structure which is monoclinic with space group *P*2/*c*. The luminescent properties of zinc tungstate have been extensively investigated because it is a widely used scintillation crystal.[2,6−8]

The studies on luminescent properties of nanosized phosphors are attracting current interests because they are significant not only for applications but also for essential understanding of nanocrystals, such as confinement effect, surface effect, etc. Among them, rare earth doped nanophosphors have attracted particular attention[9−14] because the corresponding bulk materials have large practical applications in lighting and display,[15,16] etc. It is expected that in the nanosized phosphors the luminescent quantum yield as well as the resolution of display be improved considerably. In addition, some rare earth ions such as Eu^{3+} may act as common activators to detect local environments[17] due to their super-sensitive f−f transitions. Up to now, a great number of rare earth doped nanosized phosphors have been prepared and studied,[18−20] including tungstates. In rare earth doped tungstates, tungstates emit blue-green lights themselves under ultraviolet excitation. At the same time, tungstates may also effectively transfer energy to rare earths such as trivalent europium and samarium, generating red-emissions.[21,22] Therefore, some rare earth doped tungstates become potential white-light phosphors. In the past few years, there appeared only a few literatures corresponding to the preparation and photoluminescent properties of rare earth doped tungstates nanocrystals, and their studies mainly focused on sample preparation.[22] To completely understand the luminescent properties of them, including electronic transition, energy transfer, and site symmetry, comprehensive spectral studies are required. In this paper, we mainly report the photoluminescent properties of the wolframite $ZnWO_4:Eu^{3+}$ prepared by the hydrothermal technique at different hydrothermal temperatures and different pH values. The hydrothermal synthesis of tungstates was first reported by F. Wen et al.[22] It is considered that the hydrothermal method is a more effective way than the solid-state reaction to dope Eu^{3+} ions in the lattice $ZnWO_4$ for energy transfer from WO_4^{2-} groups to Eu^{3+} ions.[22] In this paper, we observed that the central wavelength of the excitation spectra, the relative number of Eu^{3+} centers located at different symmetry sites, and the ratio of blue-green emissions to the red emissions of Eu^{3+} depended strongly on the hydrothermal conditions.

II. Experiments

A. Sample Preparation. Zinc tungstate ($ZnWO_4$) nanocrystals were prepared by the reaction of $Zn(NO_3)_2$ and $Eu(NO_3)_3$ as well as Na_2WO_4 for 12 h at different temperatures and different pH values. In a typical procedure, appropriate amounts high-purity Eu_2O_3 powder was dissolved in hot concentrated

* To whom correspondence should be addressed. E-mail: hwsong2005@yahoo.com.cn. Fax: 86-431-6176320.

10.1021/jp066712e CCC: $37.00
Published on Web 05/05/2007

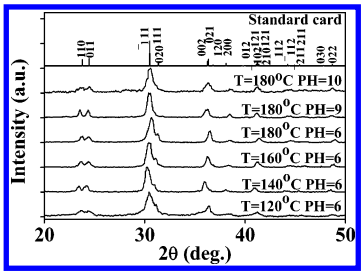

Figure 1. XRD pattern of $ZnWO_4:Eu^{3+}$ powders prepared at different hydrothermal temperatures and different pH values in comparison to the standard card.

HNO_3 to form $Eu(NO_3)_3$ solution, and $Zn(NO_3)_2 \cdot 6H_2O$ and $Na_2WO_4 \cdot 2H_2O$ were dissolved in deionzed water respectively to get the corresponding solutions. Then the later two solutions were mixed together (1 mmol $Zn(NO_3)_2$ and 1 mmol Na_2WO_4), and then appropriate $Eu(NO_3)_3$ was added with vigorous stirring. The pH value (pH = 6, 9, 10) of the mixed solution was adjusted with dropwise of HNO_3 or NaOH solution. After that, the solution was added into a Teflon-lined stainless steel autoclave of 50.0 mL capacity. The autoclave was kept at a certain temperature in the range of 120−180 °C for 12 h. Afterward the autoclave was cooled to room temperature gradually. Then the white precipitate was collected and washed with deionzed water several times. The solid was heated at 80 °C and dried under vacuum for 2 h, finally the white powders of $ZnWO_4:Eu^{3+}$ were obtained.

B. Measurements. X-ray diffraction (XRD) data were collected on a Rigaku D/max-rA X-ray diffractometer using a Cu target radiation source. Field emission scanning electron microscopy (FE-SEM) was taken on Philips LX30 electron microscopes. Fluorescence and excitation spectra were recorded at room temperature using a Hitachi F-4500 spectrophotometer equipped with a continuous 150W Xe-arc lamp. For comparison of different samples, the emission spectra were measured at a fixed bandpass of 0.2 nm with the same instrument parameters (2.5 nm for the excitation slit, 2.5 nm for the emission slit). In the measurements of high-resolution emission spectra and fluorescence dynamics, a 266 nm laser generated from a pulsed Nd:YAG (aluminum garnet) laser combined with a fourth harmonic generator was used as a pump. It was with a line width of 0.2 cm^{-1}, pulse duration of 10 ns, and repetition frequency of 10 Hz. A Rhodamine 6 G dye pumped by the same Nd:YAG laser was used as the frequency-selective excitation source. A spex 1403 spectrometer and a boxcar integrator were used to record the high-resolution emission spectra and fluorescence dynamics.

III. Results and Discussion

A. Crystal Structure and Morphology. Figure 1 shows the XRD patterns of $ZnWO_4:Eu^{3+}$ powders prepared at different hydrothermal temperatures and pH values in comparison to the standard card. It can be seen that the crystal structures of all the samples belong to the pure monoclinic phase. In comparison to the standard card, the XRD patterns of the powders became broader, indicating the formation of nanocrystals. Estimated according to Scherrer equation, the average crystalline sizes of the powders are in the range of 10−20 nm. The increasing hydrothermal temperature leads the crystalline size to increase a little.

Figure 2 shows FE-SEM images of $ZnWO_4:Eu^{3+}$ nanocrystals prepared at different conditions. It is obvious that all the powders yield nanoparticles, and they tend to aggregate together. The average size of the nanoparticles for the sample A is in the range

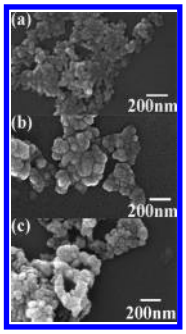

Figure 2. FE-SEM images of the $ZnWO_4:Eu^{3+}$ samples prepared at (a) 120 °C (pH = 6) (2 mol %), (b) 180 °C (pH = 6) (2 mol %), and (c) 180 °C (pH = 9) (2 mol %).

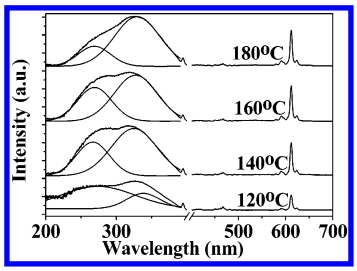

Figure 3. Room temperature excitation spectra (left part) (λ_{em} = 611 nm) and emission spectra (λ_{ex} = 326 nm) of Eu^{3+} in $ZnWO_4:Eu^{3+}$ powders prepared at different hydrothermal temperatures (right part) (pH = 6) (2 mol %).

of 40−50 nm (see Figure 2a), while that for the sample D is about 70−80 nm (see Figure 2b). This further indicates that increasing the hydrothermal temperature leads the nanoparticles to increase. Comparing the nanocrystals prepared at different pH values, we could not observe obvious change of the nanoparticles. The particle sizes observed by FE-SEM are larger than the crystalline sizes estimated by XRD patterns, which may be caused by aggregation.

B. Effect of Preparation Temperature on Luminescent Properties. Figure 3(left part) shows the excitation spectra prepared at different hydrothermal temperatures. In the spectra, the bands extending from 200 to 400 nm are dominant. The sharp line assigned to the $^7F_0-^5L_6$ transition of Eu^{3+} at 394 nm can be also observed. The broad bands can be decomposed into two Gaussian components, A and B. The location of peak A is around 260 nm, while that of peak B is around 330 nm. The two peaks have a little shift (<10 nm) in different samples. In addition, the relative contribution of the two peaks varies with hydrothermal temperature. The higher the hydrothermal temperature is, the larger the relative contribution of the peak B is. The broad bands in the UV region may contain the charge-transfer excitation of Eu^{3+} and the energy-transfer transition from tungstate groups to Eu^{3+} ions. In most of the literatures, the contribution of the two components cannot be distinguished due to spectral overlap.[22,23] The CT band corresponds to the electronic transition from the 2p orbital of O^{2-} to the 4f orbital of Eu^{3+}, and it is related closely to the covalency between O^{2-} and Eu^{3+} and coordination environment around Eu^{3+}. The decrease in energy for electron transfer in O^{2-} to Eu^{3+} represents the increase in the covalency, the decrease in ionicity between oxygen and Eu^{3+}. According to the literatures, the location of the charge-transfer band for Eu^{3+} in $ZnWO_4$ is around 250 nm.[23] In the present nanocrystals, it is suggested that the peaks A and B are both contributed by the excitation of tungstate groups, corresponding to two different crystal-field components. The corresponding emission spectra under the excitation of the same continuous Xe-lamp are shown in Figure 3 (right part). In the

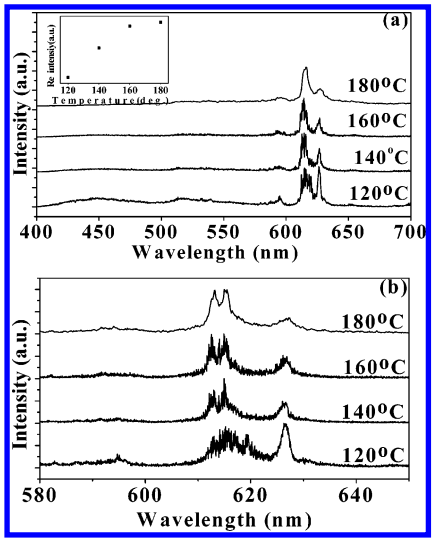

Figure 4. (a) Room temperature emission spectra of $ZnWO_4$:Eu^{3+} powders prepared at different temperatures under the 266 nm pulsed laser excitation (delay time: 5 μs). Inset: Dependence of relative integral emission intensity for Eu^{3+} ions to WO_4^2 on preparation temperatures (pH = 6) (2 mol %). (b) Emission spectra for the $^5D_0-^7F_2$ transitions (delay time: 250 μs) (pH = 6) (2 mol %).

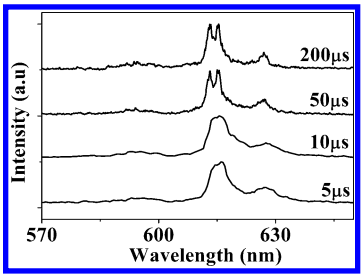

Figure 5. Time-resolved emission spectra for the $ZnWO_4$:Eu^{3+} powders (180 °C, pH = 6, 2 mol %) under 266 nm excitation.

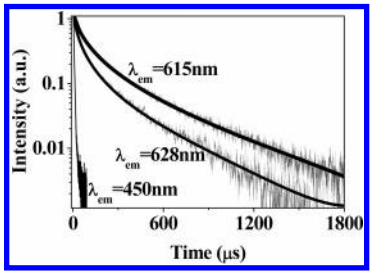

Figure 6. Fluorescence decay dynamics for the $ZnWO_4$:Eu^{3+} (2 mol %) powders (180 °C, pH = 6) measured at different wavelengths. The scattered dots are experimental data, and solid lines are fitting curves.

emission spectra, the $^5D_0-^7F_J$ transitions (J = 0, 1, 2) can be clearly observed. Among them, the electronic dipole transition of $^5D_0-^7F_2$ at 611 nm is dominant. Generally, the emission intensity of $^5D_0-^7F_J$ increases as the preparation temperature increases. As is well-known, the $^5D_0-^7F_1$ lines originate from magnetic dipole transition, while the $^5D_0-^7F_2$ lines originate from electric dipole transition. In terms of the Judd−Ofelt theory, the magnetic dipole transition is permitted. The electric dipole transition is allowed only on the condition that the europium ion occupies a site without an inversion center and is sensitive to local symmetry. Subsequently, when Eu^{3+} ions occupy inversion center sites, the $^5D_0-^7F_1$ transitions should be relatively strong, while the $^5D_0-^7F_2$ transitions should be relatively weak. The results above indicate that Eu^{3+} ions mainly occupy one site without an inversion center. Note that under the excitation of continuous lights, the band emissions caused by tungstate groups are not observed.

The high-resolution emission spectra pumped by a 266 nm pulsed laser (delay time: 5μs) are shown in Figure 4a. In the spectra, besides the $^5D_0-^7F_J$ lines (J = 0, 1, 2) for Eu^{3+} in the red range, two emission bands in the blue and green regions appear, having peaks at 450 and 519 nm, respectively, which should come from the emissions of tungstate groups. The luminescence of tungstate groups is a result of its wolframite structure. The WO_6^{2-} complex and a slight deviation from a perfect crystal structure are believed to be responsible for the emission bands, and its luminescent properties are mainly determined by the charge-transfer transitions between the O2p orbitals and the empty orbits of the central W^{6+} ions in the WO_6^{2-} complex. It is observed that the relative intensity of the $^5D_0-^7F_J$ transitions for Eu^{3+} to the bands of tungstate groups increases with increasing the preparation temperature, as shown in the inset. This could be attributed to boundary effect. It is considered that the energy of a luminescence center can only be transferred resonantly within one particle since the energy transfer is hindered by the particle boundary;[24] so a larger particle can lead to higher energy-transfer efficiency. The size of the present hydrothermal samples increase with the temperature, as mentioned above. In the $^5D_0-^7F_2$ emissions shown in Figure 4a, it can be observed that there exist two main peaks, around 615 and 625 nm, respectively. In comparison to the emission spectra in Figure 3, the relative intensity for the 625 nm peak increases. In addition, it is interesting to observe that the relative intensity increases as the hydrothermal temperature decreases. Figure 4b shows the emission spectra as the delay time is increased to 250 μs. As shown, in the samples prepared at higher temperature, the 615 nm peaks are spilt into two components further, having peaks at 613 and 615 nm, respectively. The higher the temperature is, the obvious the spectral splitting is.

Figure 5 shows time-resolved emission spectra for the $^5D_0-^7F_J$ (J = 0, 1, 2) transitions in the sample prepared at 180 °C. It is interesting to observe that corresponding to shorter delay time (5 and 10 μs), the line at 615 nm is broader. Corresponding to longer delay times (50 and 200 μs), the line at 615 nm can be identified as two components, peaking at 613 and 615 nm, respectively. This indicates that shorter delay time corresponds to larger inhomogeneous broadening. In other words, there exist at least two kinds of Eu^{3+} centers for the $^5D_0-^7F_2$ transitions. One kind of luminescent Eu^{3+} center locates at well-crystalline local environments, which demonstrates a narrower inhomogeneous width and a longer decay time constant. The other Eu^{3+} ions locate at more disordered local environments, which display a broader inhomogeneous width and a shorter decay time constant. According to the time-resolved spectra, it is possible that the energy transfer happens between Eu^{3+} centers locating at different symmetry sites or local environments.

Figure 6 shows the fluorescence dynamics (log of intensity versus time) in the $ZnWO_4$: Eu^{3+} powders (180 °C, pH = 6) measured at different wavelengths. It can be seen that for the $^5D_0-^7F_2$ transitions the fluorescence decays nonexponentially and can be divided into three different regions. In the original region the fluorescence decays quickly, in the second region the slope gradually decreases, and in the final region the slope becomes a constant again. It is a typical fluorescence dynamics in which energy-transfer process happens. Because in the system Eu^{3+} ions act as donors, it is difficult to decide the situation of the acceptors. We just consider the D−D transfer by multipolar interaction mechanism. According to theory of B. Henderson and G.F. Imbush,[26] for the D−D transfer by multipolar interaction mechanism, the luminescence decays with time as

$$I(t) = I(0)\exp[(-t/\tau_R) - (t^{3/n}/\tau_{3/n})] \quad (1)$$

with

$$1/\tau_{3/n} = \frac{4\pi}{3} n_D \Gamma\left(1 - \frac{3}{n}\right) R_{min}{}^3 (W_{0l}t)^{3/n} f_{BT} \quad (2)$$

Where τ_R is the intrinsic decay time of the excited Eu^{3+} ions, n_D is the density of donors (Eu^{3+} for our sample), $n = 6, 8, 10$ for dipole−dipole, dipole−quadrupole, and quadrupole−quadrupole mechanisms, R_{min} is the closest distance between nearest-neighbor cations, and W_{0l} is the transfer rate between Eu^{3+} ions in nearest-neighbor sites. f_{BT} is a factor to take back-transfer into account; its form depends on the model used to describe the back-transfer process. In general the dipole−quadrupole interaction is rather weak compared to the dipole−dipole interaction, so the decay curve was fitted by the above formula selecting $n = 6$. The fluorescence dynamics in the powders prepared at the other hydrothermal temperatures were also measured. The decay time constants in different samples are listed in Table 1. It can be seen that the decay time constant increased with the increasing hydrothermal temperature. In addition, it is obvious that the decay time constant measured at 628 nm is generally larger than that measured at 615 nm. In Figure 6, it can be seen that the emission for the tungstates decays exponentially, with a time constant of 4.8 μs.

C. Effect of pH Value on Luminescent Properties. The excitation spectra of the $ZnWO_4$:Eu^{3+} (2 mol %) samples prepared at 180 °C in different pH values are shown in Figure 7 (left part). It is interesting to observe that the intensity maximum in different samples varies remarkably. For the samples of pH = 10, 9, and 6, the intensity maximums locate at ~253, 279, and 327 nm, respectively. Obviously, the excitation bands in the three samples are all contributed by different components, thus they are decomposed by multi-Gaussian functions. In the sample of pH = 10, the three composed peaks locate at 253, 291, and 329 nm, respectively, while in the sample of pH = 9, they locate, respectively, at 246, 279, and 327 nm. In the sample of pH = 10, the contribution of the 253 nm peak is dominant, while in the sample of pH = 9 the contribution of the 279 nm peak is dominant. In the samples of pH = 6, the peak around 250 nm is absent and the two composed peaks locate at 276 and 330 nm. The 330 nm peak contributes dominantly. The three peaks all came from the tungstate absorption, and the peak at ~253 nm also contained the change-transfer transitions from O2p to Eu^{3+} ions.[23] The 279 and 329 nm peaks should be assigned to excitation of tungstate with different structures due to different surroundings of them, corresponding to two different tungstate groups (two kinds of W ions: W(1) and W(2)). They were the normal tungstate groups and the perturbed groups which lack one oxygen ion ascribed by M. J. J. Lammers.[27] Figure 7 (right part) shows the corresponding emission spectra. In the samples of pH = 9 and 10, the emission bands peaking at 478 nm can be clearly observed, which are assigned to the tungstate groups. In the sample of pH = 6, the 478 nm peak is absent. It is evident that as the pH value increases the luminescence of WO_4^{2-} becomes strong gradually. Therefore, changing the pH values can adjust the relative contribution of the tungstate groups (blue-green) to Eu^{3+} ions (red), thus change the color of the $ZnWO_4$:Eu^{3+}, which has potential application in the device of white-light phosphors. It is suggested that pH values affect the relative number of the perturbed tungstate groups to the normal tungstate groups. As the pH value deceased, the relative number of the perturbed tungstate groups to normal tungstate groups increased;

TABLE 1: Variation of Fluorescence Decay Constants of $ZnWO_4$:2 mol % Eu^{3+} (pH = 6) on Sample Preparation Temperature[a]

	λ_{em} = 615 nm		λ_{em} = 628 nm	
sample temp (°C)	τ (μs)	$\tau_{n/3}$ ($\mu s^{1/2}$)	τ (μs)	$\tau_{n/3}$ ($\mu s^{1/2}$)
120	362.3	16.7	486.4	6.3
140	411.5	18.0	492.6	9.4
160	531.9	16.9	411.5	10
180	409.8	14.3	454.5	8.3

[a] τ is the decay time constant of Eu^{3+}, and $\tau_{n/3}$ is the parameter defined by eq 2 in the text.

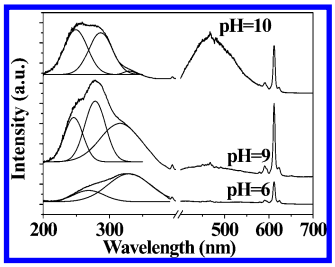

Figure 7. (a) Excitation spectra (λ_{em} = 611 nm) and (b) emission spectra of Eu^{3+} (2 mol %) for the samples synthesized the same temperature (180 °C) and at different pH values.

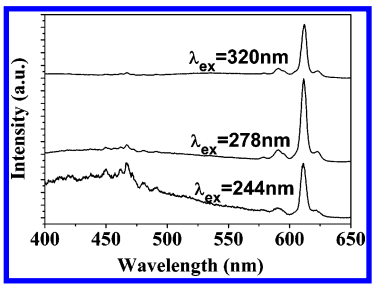

Figure 8. Emission spectra for the $ZnWO_4$:Eu^{3+} (2 mol %) powders (180 °C, pH = 9) under the excitation at different wavelengths.

as a consequence, the corresponding excitation path became more effective compared to others. The broad emission band appeared for the sample pH = 10 together with the absence of excitation band at 320 nm, implying that the charge transfer of O−Eu and O−W(1) both happened. For the sample pH = 6, when the excitation wavelength was changed to 327 nm, the second type WO_4^{2-} group was excited, subsequently, the resonant energy transfer from the second type WO_4^{2-} group to $^5H_3$ of Eu^{3+} happened, so the emission of the second type WO_4^{2-} group disappeared.

Figure 8 shows the emission spectra in the sample of pH = 9 under the excitation of different wavelengths. It is evident that corresponding to the excitation of the 246 and 279 nm bands, the emissions that originated from tungstate groups appear due to the charge transfer from O2p to W^{6+} ions, while to the excitation of the 327 nm band, these emissions disappear due to efficient resonant energy transfer from the second type WO_4^{2-} group to Eu^{3+}. On the basis of the above results, we suggest that in the $ZnWO_4$:Eu^{3+} nanocrystalline powders, the emissions for tungstate groups mainly originate from the charge transfer from excited 2p orbits of O^{2-} to the empty orbits of the central W^{6+} ions. On the other hand, the emissions for Eu^{3+} ions are contributed by both the charge transfer from O^{2-} to Eu^{3+} and the energy transfer from W^{6+} ions to Eu^{3+} ions. When the excited wavelength 244 nm was selected, the charge transfer from O2p to W^{6+} ions and from O2p to Eu^{3+} both happened. When the excited wavelength changed to ~327, only the charge transfer from O2p to the second type W^{6+} ions occurred, and

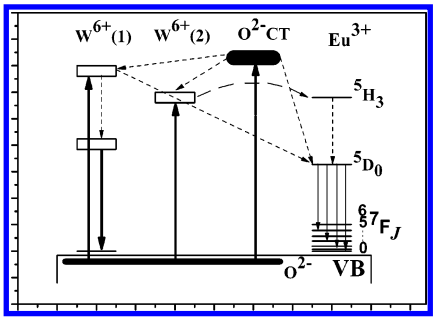

Figure 9. Schematic diagram for the luminescent processes of $ZnWO_4$:Eu^{3+} nanocrystals.

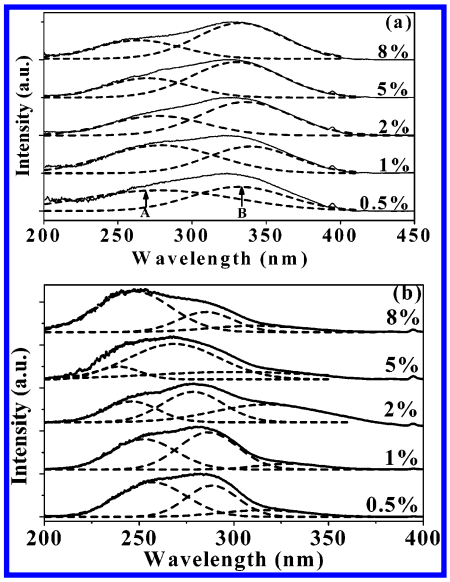

Figure 10. Excitation spectra (λ_{em} = 611 nm) for different Eu^{3+} concentration of $ZnWO_4$:Eu^{3+} powders prepared at 180 °C in different pH values: (a) pH = 6, (b) pH = 9.

then the energy was resonantly transferred to $^5H_3$ of Eu^{3+}. Accordingly, the schematic diagram of the photoluminescence processes is drawn as Figure 9.

D. Photoluminescence on Eu^{3+} Concentration. The dependence of photoluminescence properties on the concentration of Eu^{3+} is studied also. Figure 10 shows excitation spectra of Eu^{3+} in the $ZnWO_4$:Eu^{3+} powders containing different concentrations of europium and prepared at different pH values (a) pH = 6, (b) pH = 9. It can be seen that in the samples of pH = 6, the excitation bands all can be composed of two peaks, A and B. The relative contribution of the peak A to peak B has only a little variation as the concentration of europium varies. In the samples of pH = 9, the excitation spectra change considerably with europium concentration. Simplyy, the excitation bands can all be decomposed into three components, similar to the results shown in Figure 7. The contribution of the three components varies remarkably with doping concentration of europium. The higher concentration of europium leads the relative contribution at shorter wavelength to increase. As a result, the excitation maximum shifts to blue with the increasing europium concentration.

Figure 11a shows the emission spectra of the $ZnWO_4$: Eu^{3+} powders prepared at pH = 9 (180 °C) with different concentrations of europium. From the spectra it can be seen that the emissions originated from the tungstate groups vary with Eu^{3+} concentration complicatedly. First the fluorescence intensity decreases with the increasing concentration. In the 2 mol % sample, the intensity is the weakest. Presently, the origin of the complicated variation is not clarified. It is suggested that

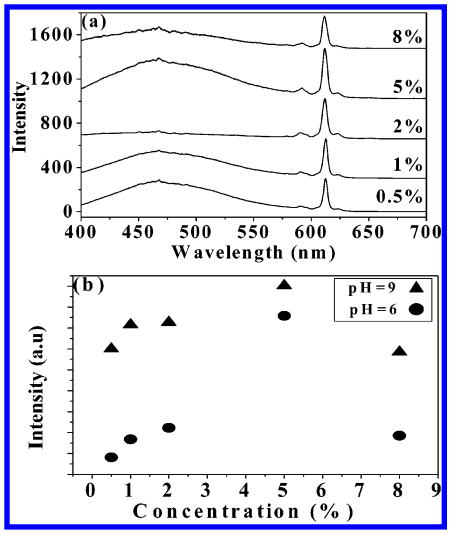

Figure 11. (a) Emission spectra of the $ZnWO_4$:Eu^{3+} powders with different concentration of europium prepared at pH = 9 (180 °C). (b) The luminescent intensity of Eu^{3+} in samples with different doping concentration pH = 6 and 9 (180 °C).

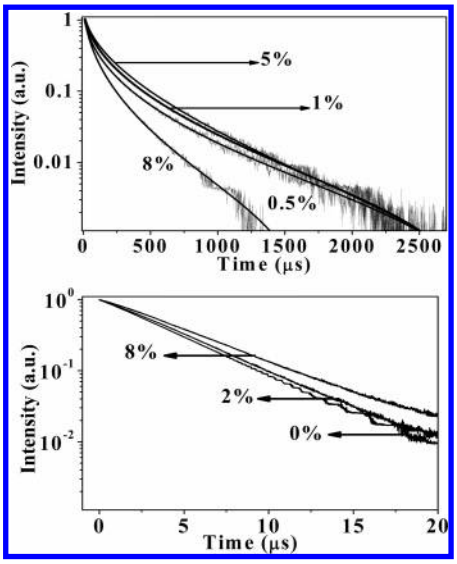

Figure 12. Fluorescence decay curves in the samples with different europium concentration: (a) $^5D_0$−$^7F_2$ transitions at 615 nm, the scattered dots are experimental data and solid lines are fitting curves, and (b) tungstate transitions at 450 nm.

in the system there exists not only the energy transfer from WO_4^{2-} to Eu^{3+} but also the back transfer from Eu^{3+} to WO_4^{2-}. The existence of these two reverse processes leads the intensity of WO_4^{2-} to vary complicatedly. Figure 11b shows the emission intensity of $^5D_0$−^7F_J for Eu^{3+} as a function of europium concentration. In the sample series with pH = 6 and pH = 9, the optimum values of europium concentration are both 5 mol %.

Figure 12a shows the fluorescence decay dynamics for Eu^{3+} in the $ZnWO_4$ powders with different concentrations of europium. It is obvious that in all the samples the florescence decays nonexponentially, and the curve can be fitted also by formula 1. Figure 12b shows the fluorescence decay dynamics for the emission of tungstate in the corresponding samples. As can be seen that, the fluorescence decays fast and exponentially. The fluorescence decay time constants in the samples with different Eu^{3+} content are listed in Table 2. It was obvious that the fluorescence decay time constants of Eu^{3+} decreased with the increasing Eu^{3+} content. That was caused by the cross-

TABLE 2: Variation of Decay Time Constants of Eu^{3+} and WO_4^{2-} in the Samples Prepared at pH = 6 and T = 180 °C on Europium Concentration[a]

Eu content (%)	τ (μs)	$\tau_{n/3}$ ($\mu s^{1/2}$)	τ_T (μs)
0			4.5
0.5	534.8	11.7	4.8
1.0	483.1	14.7	4.7
2.0	409.8	14.3	4.8
5.0	427.4	18.4	4.9
8.0	215.1	12.3	5.4

[a] τ is the decay time constant of Eu^{3+}, $\tau_{n/3}$ is the parameter defined by eq 2 in the text, and τ_T is the decay time constant of the WO_4^{2-}.

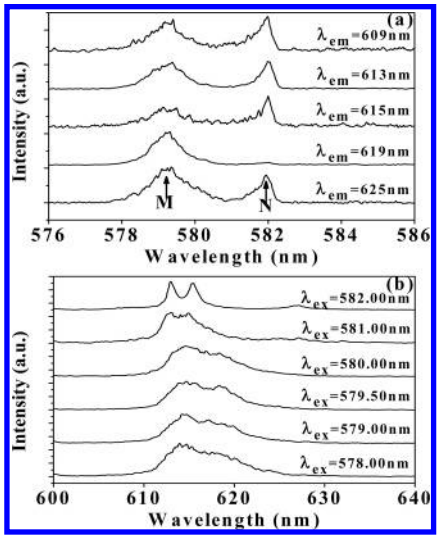

Figure 13. (a) Room temperature $^7F_0-^5D_0$ excitation spectra monitoring different $^5D_0-^7F_2$ sites, (b) $^5D_0-^7F_2$ emission spectra selectively exciting $^7F_0-^5D_0$ transitions in sample $ZnWO_4$:Eu^{3+} (2 mol %), prepared at 180 °C (pH = 6).

relaxation among Eu^{3+} ions. As for the fluorescence decay of the tungstate emission: the more the concentration of europium is, the slower the fluorescence decays. This could be attributed to the influence of Eu^{3+} doping on some defect states. The decrease of defect states will lead the nonradiative transition to decrease, as a consequence the fluorescence lifetime increases.

E. Site Symmetry. The site symmetry surrounding Eu^{3+} ions in the $ZnWO_4$:Eu^{3+} nanocrystals was studied by frequency-selective excitation spectra. Parts a and b of Figure 13show, respectively, room temperature $^7F_0-^5D_0$ excitation spectra monitoring different $^5D_0-^7F_2$ sites, and the $^5D_0-^7F_2$ emission spectra selectively exciting $^7F_0-^5D_0$ transitions in the sample $ZnWO_4$:Eu^{3+} (2 mol %), prepared at 180 °C (pH = 6). In Figure 13a, two excitation peaks are distinguished, located at 579 at 582 nm, respectively. Generally, the $^5D_0-^7F_0$ transition of Eu^{3+} is a parity forbidden, but when Eu^{3+} occupy one of *Cs*, *Cn*, *Cnv*, the parity forbidden will be partially permitted and thus a $^5D_0-^7F_0$ emission can be observed. Because the $^5D_0-^7F_0$ line has no splitting at any crystal-field, it is suitable to study the site symmetry surrounding Eu^{3+}. The observation of two $^7F_0-^5D_0$ excitation peaks indicate that there exist two luminescent symmetry sites, which are labeled as site M and site N, respectively. It can be seen that the line at 579 nm (site M) is broader than the line at 582 nm (site N). In Figure 4b, it can be seen that corresponding to the excitation at site N, there appear two distinctive $^5D_0-^7F_2$ lines, at 613 and 615 nm, respectively, while corresponding to the excitation at site M there appears only one broader line due to spectral overlapping of the two lines. Comparing to the time-resolved emission spectra in Figure 5, we could conclude that the emissions of Eu^{3+} at site M correspond to a shorter decay time constant, while those at site N to a longer constant.

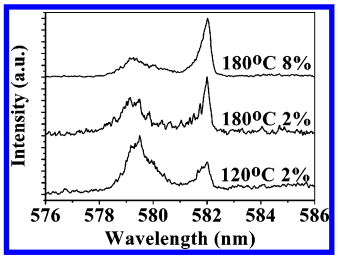

Figure 14. Room temperature $^7F_0-^5D_0$ excitation spectra monitoring different $^5D_0-^7F_2$ sites in sample $ZnWO_4$:Eu^{3+} (2 mol %) prepared at 120 °C (pH = 6), (2 mol %) 180 °C (pH = 6), and (8 mol %) 180 °C (pH = 6).

The site-selective excitation experiments were also performed in the other samples. Figure 14 shows a comparison of the frequency-selective excitation spectra in different samples. It is apparent that as the preparation temperature decreases (corresponding to smaller particle size), the relative contribution for the emissions of Eu^{3+} ions at site M increases, while as the doping concentration of europium increases, the relative contribution for site N increases. Therefore, we can conclude that the emissions of Eu^{3+} at site M have the following features in comparison to site N: (1) It locates at the higher energy side of the emission at site N. (2) It is with a broader inhomogeneous width and with a shorter decay time constant. (3) The contribution of the emission increases with decreasing particle size. These are typical features for the emissions of Eu^{3+} locating at the surface or near the surface according to our previous studies in Y_2O_3:Eu^{3+} nanocrystals;[25] thereby, the emission of Eu^{3+} at symmetry site M is attributed to photoluminescence of Eu^{3+} at the surface site, while that at site N to the luminescence at the inner site. In comparison to the results with different europium concentrations, the relative contribution of inner site (N) became larger, as the europium concentration increased.

IV. Conclusions

We have synthesized and characterized the $ZnWO_4$:Eu^{3+} nanocrystals prepared by hydrothermal method, and systematically studied the dependences of luminescence properties on various preparing conditions, such as hydrothermal temperature, pH value, and doping concentration of europium. The results demonstrate the following: (1) The particle size of the nanocrystals grows with increasing hydrothermal temperature, while it rarely changes with pH value. (2) The excitation bands for Eu^{3+} are contributed by three components, including the charge-transfer transition band from O^{2-} to Eu^{3+} and O^{2-} to W^{5+} (~250 nm) and two energy-transfer transition bands from the tungstates to Eu^{3+} (~280 and ~330 nm). The relative contributions of these different components vary a little with hydrothermal temperature and concentration of europium, but vary significantly with pH value. A larger pH value leads the central wavelength to shift blue. (3) The blue-green emission bands caused by the tungsate groups can be observed at room temperature, and the relative intensity of the blue-green emission bands to the red emissions of $^5D_0-^7F_2$ for Eu^{3+} can be considerably modified by changing the pH value. By this way, the white color phosphors can be obtained. (4) According to the studies of time-resolved emission spectra, there exist $^5D_0-^7F_2$ emissions of Eu^{3+} surrounding two local environments, better crystalline and more disordered. The lines corresponding to the former local environment are sharper and decay slower,

while the lines corresponding to the latter local environment are broader and decay faster. The site-selective excitation spectra further indicate that they correspond to two different symmetry sites of Eu^{3+} ions, respectively the inner site and the surface site. (5) The emissions for tungstate groups mainly originate from the charge transfer from excited 2p orbits of O^{2-} to the empty orbits of the central W^{6+} ions. On the other hand, the emissions for Eu^{3+} ions are contributed by both the charge transfer from O^{2-} to Eu^{3+} and the energy transfer from W^{6+} ions to Eu^{3+} ions. In conclusion, this work is helpful in completely understanding the luminescent properties of nanocrystalline $ZnWO_4$:Eu^{3+} powders.

Acknowledgment. This work is supported by the National Nature Science Foundation of China (Grants 10374086 and 10504030) and Talent Youth Foundation of JiLin Province (Grant 20040105).

References and Notes

(1) Chamberland, B.; Kafalas, J.; Goodenough, J. *Inorg. Chem*. **1977**, *16*, 44.
(2) Takagi, T.; Fukazawa, J. *Appl. Phys. Lett.* **1980**, *36*, 278.
(3) Uitert, L.; Preziosi, S. *J. Appl. Phys*. **1962**, *33*, 2908.
(4) Wang, H.; Medina, F.; Zhou, Y.; Zhang, Q. *Phys. Rev. B* **1992**, *45*, 10356.
(5) Tanaka, K.; Miyajima, T.; Shirai, N.; Zhang, Q.; Nakata, R. *J. Appl. Phys*. **1995**, *77*, 6581.
(6) Pisarevskii, Y.; Silvestrova, L.; Voszka, R.; Peter, A. *Phys. Rev. B* **1990**, *43*, 10356.
(7) Born, P.; Robertson, D.; Smith, P.; Hames, G.; Reed, J.; Telfor, J. *J. Lumin.* **1981**, *24/25*, 131.
(8) Grassmann, H.; Moser, H. *J. Lumin*. **1985**, *33*, 109.
(9) Meyssamy, H.; Riwotzki, K. *Adv. Mater*. **1999**, *11*, 840.
(10) Yada, M.; Mihara, M.; Mouri, S.; Kijima. *Adv. Mater*. **2002**, *14*, 309.
(11) Wang, X.; Li, Y. *J. Eur. Chem*. **2003**, *9*, 5627.
(12) Meltzer, R.; Feofilov, S.; Tissue, B. *Phys. Rev. B*. **1999**, *60*, 14012.
(13) Williams, D.; Bihari, B.; Tissue, B.; McHale, J. *J. Phys. Chem. B*. **1998**, *102*, 96.
(14) Song, H.; Chen, B.; Peng, H.; Zhang, J. *Appl. Phys. Lett*. **2002**, *81*, 1776.
(15) Shin, J.; Hoven, G.; Polman, A. *Appl. Phys. Lett*. **1995**, *66*, 2379.
(16) Fu, M.; Yoshida, M.; Kanzawa, Y.; Hayashi, S.; Yamamoto, K. *Appl. Phys. Lett*. **1997**, *77*, 1198.
(17) Song, H.; Yu, L.; Lu, S.; Wang, T.; Liu, Z.; Yang, L. *Appl. Phys. Lett*. **2004**, *85*, 470.
(18) Yu, L.; Song, H.; Lu, S.; Liu, Z.; Yang, L. *Chem. Phys. Lett*. **2004**, *399*, 384.
(19) Wu, C.; Qin, W.; Qin, G.; Zhao, D.; Zhang, J.; Huang, S. *Appl. Phys. Lett*. **2003**, *82*, 520.
(20) Jia, C.; Sun, L.; Luo, F.; Jiang, X.; Wei, L.; Yan, C. *Appl. Phys. Lett.* **2004**, *84*, 5305.
(21) Treadaway, M.; Powell, R. *Phys. Rev. B* **1975**, *15*, 862.
(22) Wen, F.; Zhao, X.; Huo, H.; Chen, J.; Lin, E.; Zhang, J. *Mater. Lett*. **2002**, *55*, 152.
(23) Shigeo, S.; William, M. *Phosphor Handbook*; CRC Press: Washington, DC, 1998.
(24) Wei, Z.; Sun, L.; Liao, C.; Yin, J.; Jiang, X.; Yan, C. *J. Phys. Chem. B*. **2002**, *106*, 10610.
(25) Peng, H.; Song, H.; Chen, B.; Lu, S.; Huang, S. *Chem. Phys. Lett*. **2003**, *370*, 485.
(26) Henderson, B.; Imbusch, G. F. *Optical Spectroscopy of Inorganic Solids*; Oxford University Press (USA): New York, 2006.
(27) Lammers, M. J. J.; Blasse, G.; Robertson, D. S. *J. Lumin.* **1981**, *63*, 569.